GEOLOGIJA *55/1*, 93–106, Ljubljana 2012

doi:10.5474/geologija.2012.007

Mineral chemistry of monazite-(Nd), xenotime-(Y), apatite, fluorite and zircon hosting in lamprophyre dyke in Abu Rusheid area, South Eastern Desert, Egypt

Mohamed A. ALI

Nuclear Materials Authority P. O. Box: 530 El-Maadi, Cairo, Egypt; e-mail: dr_mohamed1966@yahoo.com

Prejeto / Received 14. 3. 2011; Sprejeto / Accepted 30. 3 2012

Key words: Mineralized lamprophyre dyke, REE-minerals, REE-bearing minerals, mineral chemistry, South Eastern Desert, Egypt.

Abstract

The studied mineralized lamprophyre dyke in Abu Rusheid area is trending NNW-SSE, and occurs within Abu Rusheid mineralized shear zone, measuring 0.2 - 1.0 m in width and 0.5 - 1.0 km in length. It was emplaced parallel with the Abu Rusheid shear zone. The dyke is mainly composed of plagioclases, amphiboles, mica (muscovite and biotite), relics of pyroxenes with K-feldspars and quartz derived from surrounding country rocks as phenocrysts embedded in fine-grained groundmass. The lamprophyre dyke hosts REE-minerals monazite-(Nd), xenotime-(Y), and REE-bearing minerals apatite, fluorite, zircon-(Hf), rutile with inclusions of xenotime and iron oxides. The emplacement of lamprophyre dyke caused heating in the mineralized shear zone of Abu Rusheid area. The lamprophyre dyke was subsequently affected by hydrothermal alterations (e.g. chlorite-carbonate, muscovitization, fluoritization). The REE were remobilized from the mineralized shear zones by hydrothermal solutions and re-precipitated as REE-minerals xenotime-(Y) and monazite-(Nd) around flourapatite, fluorite, zircon and rutile. The solid solutions between monazite-(Nd) and xenotime-(Y) were formed as a product precipitation from hydrothermal solutions. Also, the apatite mineral in the lamprophyre dyke was subjected to the heating during the emplacement, which lead to its alteration and breakdown with concominant precipitation of xenotime-(Y) and monazite-(Nd). The chemistry of monazite-(Nd) and xenotime-(Y) obtained by scanning electron microscopy (SEM), and electron probe microanalysis (EPMA), showed that these minerals are enriched in U and Th. The monazite-(Nd) associated with fluorapatite in the studied dyke is poor in Th ($0.02 \leq Th \leq 0.81$ wt%), but usually rich in U ($0.92 \leq U \leq 2.91$ wt%), which indicates that monazite formed as a result of flourapatite metasomatism.

Introduction

The Abu Rusheid area is one of the most important areas in the South Eastern Desert of Egypt, especially in rare-metal mineralization and is included in wadi Sikait and wadi El Gemal area. It lies about 97 km southwest of Marsa Alam town and is accessible from the Red Sea through wadi El-Gemal desert track (Fig. 1).

The area is located in the huge fault systems of Sikait-Nugrus environ. The age of the leucogranites in the Sikaite-Nugrus (Abu Rusheid granites) area is 610 ± 20 Ma determined by Rb-Sr method (Moghazi et al., 2004). The Abu Rusheid area lies to the NE of the major shear zone known as the Nugrus thrust fault (Greiling et al., 1988) or Nugrus strike-slip fault (Fritz et al., 2002). This shear zone separates high-temperature metamorphic rocks of the Hafafit complex in the SW from mainly low grade ophiolitic and arc volcanic assemblages to the NE (Bennett & Mosley, 1987). Shear zones are known to form important mechanical weaknesses that affect the geology of the continental lithosphere as a kinematic response to deformation (Butler et al., 1995). Greiling et al. (1993) believe that shear zones in the Pan African basement of the Eastern Desert may be related to compressional, as well as extensional stresses; however, both types of deformation led to antiformal structures on a regional scale. Abdel-Monem & Hurely (1979) estimated the age date of psammitic gneisses by zircon detrital age, which ranges between 1120 Ma and possibly 2060 Ma suggesting that this basement may be the so called Nile Craton.

Hassan (1964) studied geology and petrography of the radioactive minerals and rocks in wadi Sikait and wadi El Gemal area. Also, Hassan (1973) and Hilmy et al. (1990) studied geology, geochemistry and mineralization of radioactive columbite-bearing psammitic gneisses of wadi Abu Rusheid. El-Gemmizi (1984), Saleh (1997) and Ibrahim et al. (2004) studied the Abu Rusheid area and recorded several types of mineralization, such as Ta-Nb minerals, zircon, thorite, and secondary uranium minerals. Raslan (2005) identified columbite, Hf-rich zircon and dark Li-mica (zinnwaldite) in Abu Rusheid mineralized gneiss. The latter author has further been able to identify mineral ishikawaite in Abu Rusheid minera-

lized gneiss (Raslan, 2008). Dawood (2010) studied the mineral chemistry and genesis of uranyl minerals associated with psammitic gneisses of Abu Rusheid area, and concluded that the composition and genesis of uranyl mineralization provide additional information about the behavior of radionuclides in arid environments and at very oxidizing conditions. Ali et al. (2011) studied the mineralogy and geochemistry of Nb-, Ta-, Sn-, U-, Th-, and Zr-bearing granitic rocks in Abu Rusheid shear zones, and proved, on the basis of field evidence, textural relations, and compositions of the ore minerals, that the main mineralizing event was magmatic (629 ± 5 Ma, CHIME monazite), with later hydrothermal alteration and local remobilization of high-field-strength elements.

Ibrahim et al. (2007a) recorded the occurrence of REE up to (1.5 %) in the studied lamprophyre dykes. Also, Ibrahim et al. (2007b) studied the base-metal mineralization hosting uranium and geochemistry of the lamprophyres within the shear zones of Abu Rusheid area.

The present study shows the detailed mineral chemistry of REE-minerals (monazite-(Nd), xenotime-(Y)) and REE-bearing minerals (apatite, fluorite, and zircon) within mineralized lamprophyre dyke, and also discusses the genesis of these minerals.

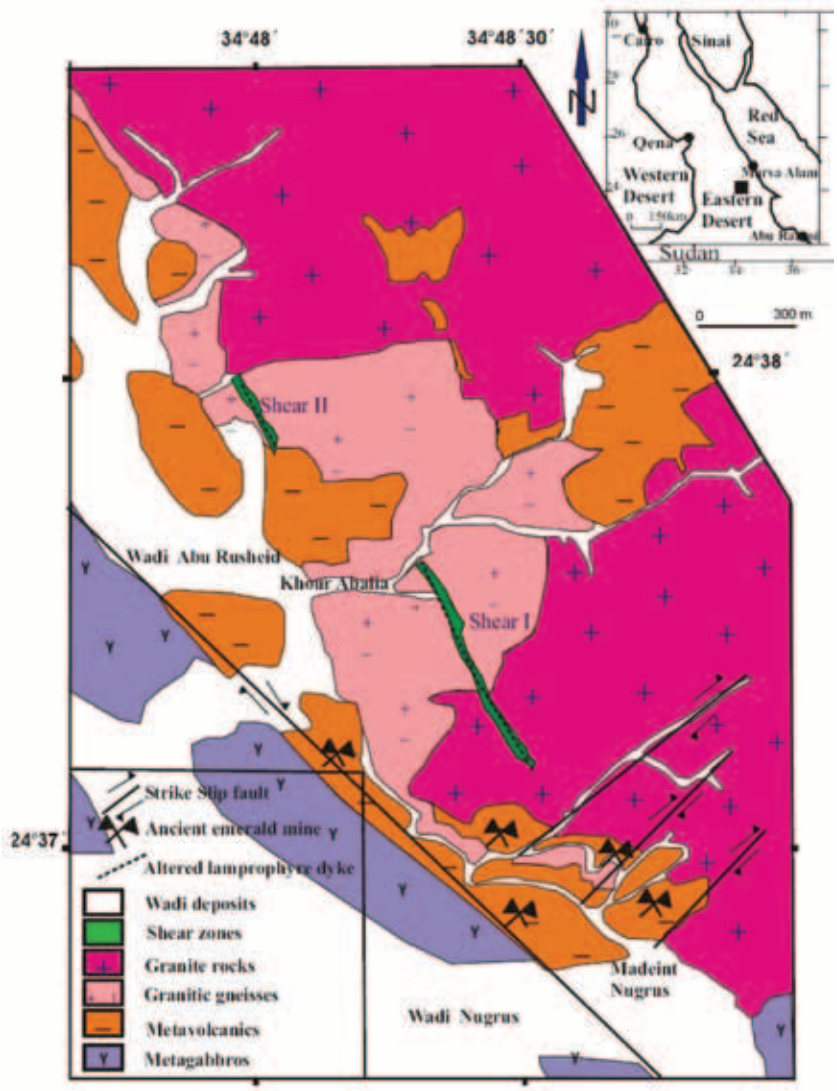

Fig. 1. Geological map of Abu Rusheid area showing the studied altered lamprophyre dyke, cutting mineralized shear zone (modified after Ibrahim et al. 2004).

Geological setting

The basement rocks sequence of the Precambrian rocks at Abu Rusheid area are arranged as follows: (1) ophiolitic mélange, consisting of ultramafic rocks and layered metagabbros with a metasedimentary matrix; (2) cataclastic rocks (peralkalic granitic gneisses) in the core of the granitic pluton, which are composed of protomylonites, mylonites, ultramylonites, and silicified ultramylonites, (3) mylonitic granites; and (4) post-granitic dykes and veins (Ibrahim et al., 2004). The rare-metal peralkalic granitic gneisses and cataclastic to mylonitic rocks (Ali et al., 2011) are highly foliated and contain primary mineralization of uraninite, thorite and zircon minerals. These rocks are intruded by two mica (muscovite-biotite) granites. The cataclastic rocks are crosscut by NNW-SSE trending altered and mineralized shear zone with >1 km in length and 0.5 - 5 m in width (Fig.1).

The lamprophyre dyke of 0.2 - 0.5 m in width and > 1 km in length was emplaced along the altered and mineralized shear zone. Lamprophyre dyke is fine-to medium-grained, highly fractured parallel to the mineralized shear zone and characterized by dark grayish to black colors. Iron oxides, fluorite and carbonatite are present as

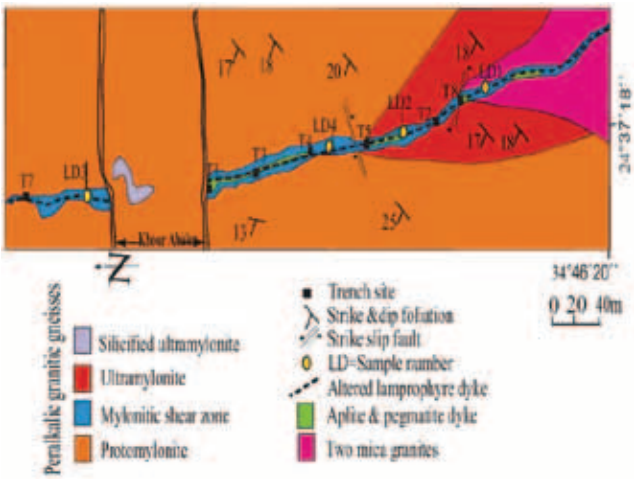

Fig. 2. Sketch map of the shear zone I shwing the studied altered lamprophyre dyke, and sampling locations (), (modified after Ibrahim et al. 2007a).

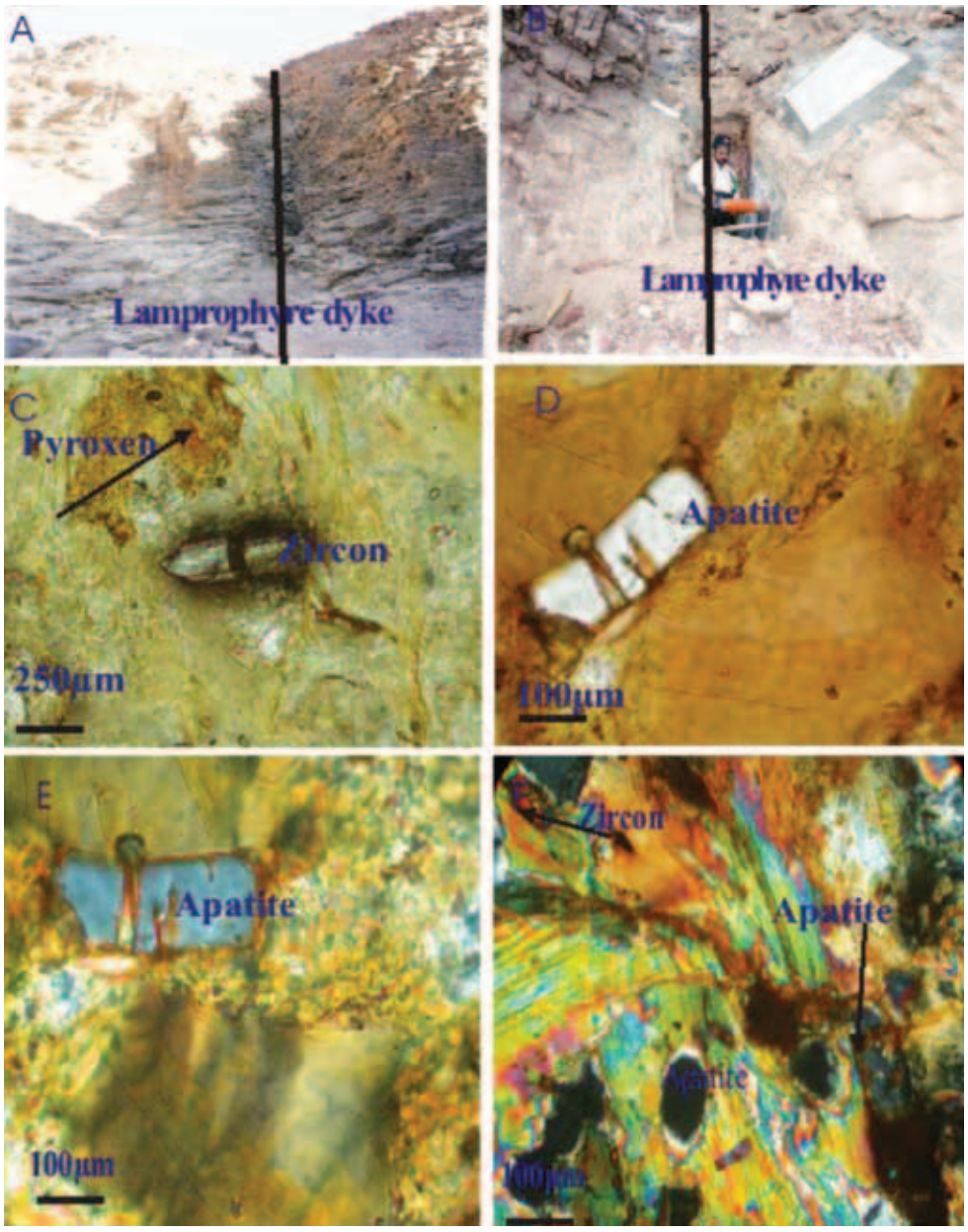

Fig. 3 a) Photo of NNW-SSE trending of lamprophyre dyke in the Abu Rusheid area, b) detailed photo of the lamprophyre dyke cuting the mineralized shear zone in the Abu Rusheid area, c) The pyroxene is altered to amphiboles and iron oxides, notice large zircon crystal within lamprophyre dyke, d) large apatite crystal in the P. L. (Polarized Light), e) and under C. N. (Crossed Nichols), and f) numerous crystal of apatite and zircon associated with muscovite and iron oxides (P. L.).

fillings in fracture planes. The studied dyke is completely altered and cross-cuts rare-metal peralkalic granitic gneisses and cataclastic mylonitic rocks in the Abu Rusheid mineralized shear zone in the direction of NNW-SSE (Figs. 2, 3b).

Petrographically, the altered lamprophyre dyke is mainly composed of plagioclases, amphiboles, relics of pyroxenes and secondary muscovite after biotite. The pyroxene is altered to amphiboles and iron oxides (Fig. 3c), while the biotite is altered to muscovite and iron oxides. K-feldspars and quartz are found in the lamprophyre dyke as phenocrysts embedded in the fine-grained groundmass. They were formed from xenoliths and relics of mineralized shear zone (granitic gneisses). Numerous apatite and zircon crystals, associated with muscovite and iron oxides were found. Apatite, fluorite, monazite, xenotime and zircon occur as accessory minerals (Fig. 3d to f). Carbonate, chlorite, epidote, sericite, iron oxides and muscovite are secondary minerals.

REE-minerals and REE-bearing minerals

Due to their large ionic radii and charge, the REE, as well as U and Th, behave incompatibly during magmatic processes. The LREE tend to be concentrated in highly fractionated basic rocks, such as carbonatites (Förster, 2000), whereas HREE and especially Y tend be concentrated in fractionated acidic rocks, such as alkaline granites and pegmatites. Concerning the heavy REE (HREE), Hanson (1978) invoked zircon as the major source of HREE in granitic rocks, while Jefferies (1984) considered partitioning of HREE between zircon, xenotime, and apatite. Mineyev (1963) reported that the HREE can easily form sodium fluoro-complexes (e.g., $Na(REE)F_4$) under hydrothermal conditions. These complexes from preferably with HREE of smaller ionic radii (Humphris, 1984).

The crystal structures of many of REE-minerals are poorly known because the phases are metamict in nature (Th and U commonly sub-

stitute for REE in minerals, as mentioned above). The smaller HREE, or Y-group, exhibits irregular coordination numbers with oxygen most commonly of 8, whereas the larger light REE (LREE), or Ce-group, exhibits larger coordination numbers, most commonly of 9 (e.g., Miyawaki & Nakai, 1987). The LREE have relatively large ionic radii similar to those of Ca^{2+} and Th^{4+}. The trivalent LREE (Ce-group) are very similar crystal-chemically to Ca^{2+}, and they commonly substitute for Ca in rock-forming minerals. Substitution of a trivalent REE cation for divalent Ca is achieved by compensation of charge through a coupled substitution.

The REE-orthophosphate minerals monazite and xenotime are known from a wide range of magmatic (Bea, 1996; Förster, 1998a, b; Viskupic & Hodges, 2001) and metamorphic rocks (Heinrich et al., 1997), especially rocks characterized by mildly to strongly peraluminous compositions. Monazite (LREE(PO_4)) is a monoclinic mineral, with the space group $P2_1/n$, which is isostructural to huttonite, the high-P high-T polymorph of $ThSiO_4$. The most common of the monazite series is monazite-(Ce), which is widespread in granites (mainly S-type), alkaline rocks (syenites, carbonatites), pegmatites, metapelites to metapsammites, hydrothermal veins or occurs as authigenic mineral in clastic sediments. Monazite-(La), monazite-(Nd), and monazite-(Sm) occur less frequently (Graeser & Schwander, 1987; Gaines et al., 1997; Anthony et al., 2000; Massau et al., 2002). Xenotime (Y, HREE(PO_4)) is tetragonal, with the space group $I4_1/amd$, and is isostructural to thorite, which is the low-P low-T polymorph of $ThSiO_4$ (Pabst & Hutton, 1951). Both atomic arrangements are based on chains of alternating phosphate tetrahedra and REE polyhedra along [001] where the REE ions are 8-fold coordinated in xenotime and 9-fold in monazite (Ni et al., 1995). Minor emphasis has been given to xenotime, which also incorporates relatively high amounts of U and, to a minor extent, also Th. It is known from natural assemblages (Franz et al., 1996) that Th and U are incorporated in monazite and xenotime by two exchange mechanisms. In natural rocks, coexisting monazite-xenotime pairs suggest that Th is preferentially incorporated into monazite as brabantite ($CaTh(PO_4)$) (Rose, 1980) and U into xenotime as coffinite ($USiO_4$) component (Franz et al., 1996); however, quantitative relationships are unknown. Andrehs & Heinrich (1998) found that the monoclinic structure preferentially incorporates the LREE, whereas the tetragonal structure incorporates preferentially the HREE.

Zircon is an important member of REE-bearing minerals and a common accessory mineral in plutonic igneous rocks, especially those of granite group. It is generally present as small early formed crystals often enclosed in later minerals, but may form large well developed crystals in granites and pegmatites (Deer et al., 1966). Hussein (1978) and Abadalla et al. (2008) stated that the radioactive zircons are usually zoned. The radioactive zircon is also characterized by metamictization. The explanation for the origin of the "Metamict State" is that the internal order of the originally crystalline form has been destroyed by α-particles bombardment from radionuclides within the structure. Zircon may be partially or completely modified giving amorphous zircon with a more isotropic character. Such minerals are called metamict zircon.

Analytical methods

Four samples of the altered lamprophyre dyke were studied in detail using optical microscopy, scanning electron microscopy (SEM), and electron probe microanalysis (EPMA). Polished thin sections were studied under reflected and transmitted light of an optical microscope in order to determine mineral associations and paragenesis. Backscattered electron images (BEI) were collected with the scanning electron microscope (JEOL 6400) at the Microscopy and Microanalyses Facility, University of New Brunswick (UNB), New Brunswick, Canada. Chemical compositions of minerals were determined on the JEOL JXA-733 Super probe at 15 kV, a beam current of 50 nA and peak counting times of 30 second for all elements. Standards used for the EPMA analysis were jadeite, kaersutite, quartz, and apatite for Na, Al, Si, and P, and Ca, respectively, $SrTiO_3$ for Ti, CaF_2 for F, pure metals were used for Fe, Nb, Hf, Ta, Sn, Th, and U, YAG for Y, cubic zirconia for Zr, (La, Ce, Nd, Sm, Pr, Er, Gd, Eu, Tb, Dy, and Yb)-bearing Al-Si glass for La, Ce, Nd, Sm, Pr, Er, Gd, Eu, Tb, Dy, and Yb and crocoite for Pb.

Mineralogical investigations

Results of detailed mineralogical examination of REE-minerals and REE-bearing minerals in altered lamprophyre dyke are briefly presented in the following sections.

REE-minerals

Monazite-Nd ((Nd, Ce, La, Sm, Th)PO_4)

Monazite-(Nd) occurs as euhedral to subhedral crystals in mineralized lamprophyre dyke in the Abu Rusheid area. The monazite crystals are generally light gray in color and range in size from 5 to 30 μm (Fig. 4a, c). Monazite was found associated with iron oxides and xenotime, rimming apatite and fluorite, as inclusions in the zircon, and in the fractures and fissure track in the dyke. Monazite in the studied lamprophyre dyke is frequently heterogeneous. This means that the same crystal of monazite consists of two distinct parts; which appear dark gray and light gray in SEM (BEI) images (Figs. 5c,d). Chemical composition of these distinct parts in monazite,

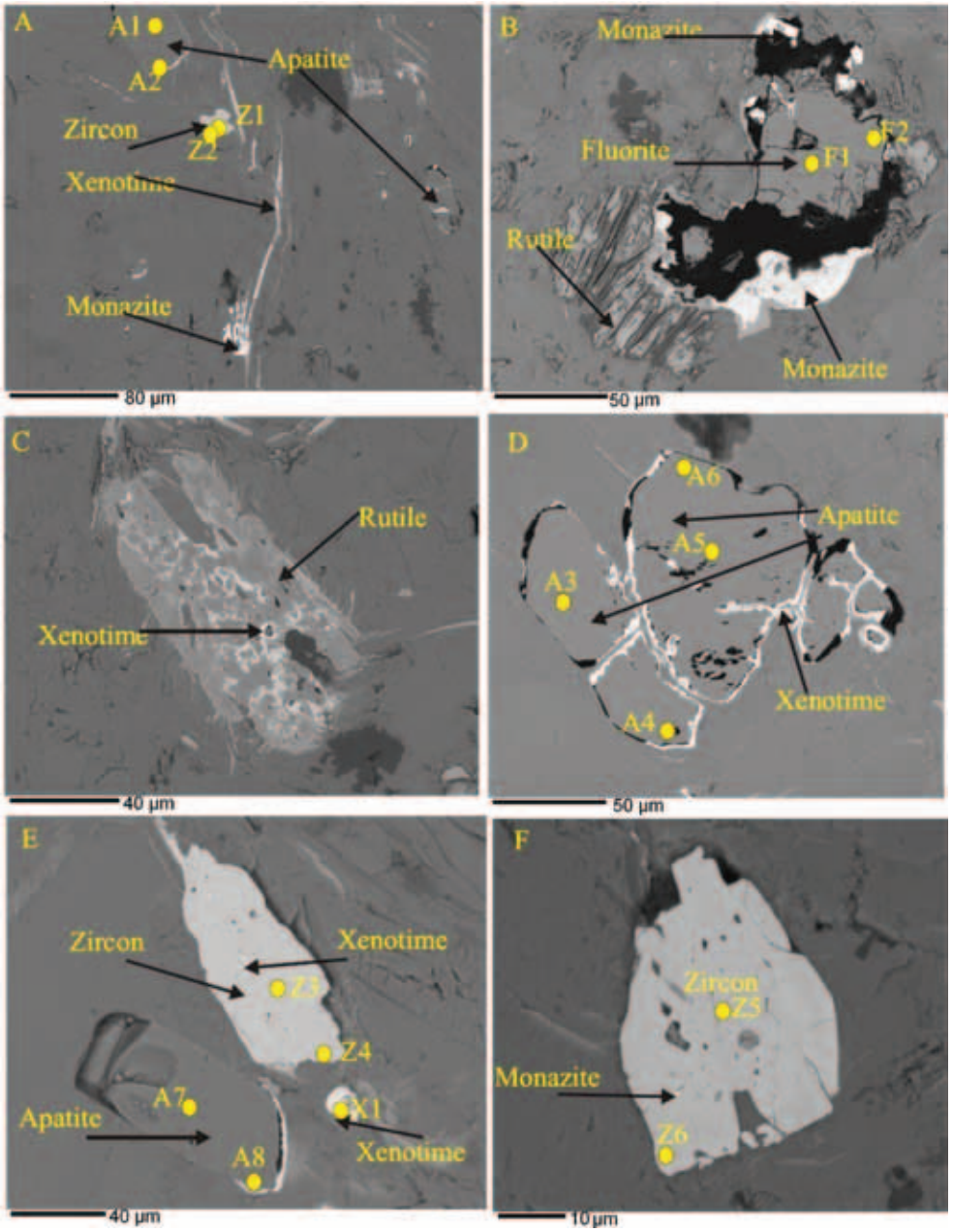

Fig. 4. SEM-BSE images of a) monazite and xenotime minerals filling fractures and fissures in the lamprophyre dyke, b) fluorite associated with monazite and rutile, c) rutile with inclusions of xenotime in the lamprophyre dyke, d) large euhedral apatite rimmed by xenotime, and e) and f) zircon with inclusions of xenotime and monazite.

obtained by the EPMA analysis, are given in Table 1 and shown in Figures 6 and 7. The results showed that contents of the major oxides in the darker part of monazite are: P_2O_5 (22.99 to 26.11 wt%), Nd_2O_3 (12.72 to 19.73 wt%), Ce_2O_3 (2.31 to 16.37 wt%), La_2O_3 (3.02 to 4.23 wt%), Pr_2O_3 (5.15 to 6.30 wt%), Sm_2O_3 (3.75 to 4.59 wt%), Gd_2O_3 (3.82 to 4.75 wt%), Dy_2O_3 (5.45 to 6.18 wt%), ThO_2 (0.02 to 0.21 wt%), UO_2 (0.71 to 1.18 wt%), while the lighter part consists of P_2O_5 (20.40 to 24.26 wt%), Nd_2O_3 (13.01 to 17.12 wt%), Ce_2O_3 (10.18 to 16.42 wt%), La_2O_3 (3.30 to 6.15 wt%), Pr_2O_3 (3.46 to 4.68 wt%), Sm_2O_3 (0.97 to 2.96 wt%), Gd_2O_3 (2.94 to 4.01 wt%), Dy_2O_3 (5.05 to 6.16 wt%), ThO_2 (0.21 to 0.81 wt%), UO_2 (0.92 to 2.91 wt%). It can be inferred from these results that the darker part of monazite-(Nd) is enriched in HREE and depleted in LREE, Th, and U; while the lighter part is depleted in HREE, Y and Ca, and enriched in Th and U. Monazite and xenotime in the Abu Rusheid lamprophyre dyke also occur in the monazite-xenotime solid solution, which indicates presence of hydrothermal solutions enriched in REE, Y, P, U, F, and Zr. The emplacement of the lamprophyre dyke in the mineralized shear zone heated the wall rocks of the shear zone, which enriched in REE, Y, P, U, F, and Zr. These elements were remobilized by hydrothermal solutions and re-precipitated in the fractures and fissure tack in the lamprophyre dyke as REE-minerals, such as monazite-(Nd), xenotime-(Y) and REE-bearing minerals, such as apatite, fluorite, zircon, rutile with inclusions of xenotime and iron oxides.

Hydrothermal and igneous monazite can be distinguished by the ThO_2 content, which is generally < 1 wt% for hydrothermal monazite and 3 to > 5 wt% for igneous monazite (Schandl & Gorton, 2004). Also, monazites formed under high-grade metamorphic conditions show a wide range of ThO_2 concentrations and are strongly zoned with respect to Th. The studied monazite is relatively heterogeneous and strongly zoned

with respect to Th. The Th content in the studied monazite is low and is consistent with its hydrothermal origin (Table 1).

Xenotime-Y ((Y, HREE)PO_4)

Xenotime in lamprophyre dykes occurs as euhedral to subhedral crystals associated with apatite, monazite, rutile, fluorite, and zircon minerals. In places, it can also be found as anhedral rims around apatite, fluorite and rutile. In the altered lamprophyre dykes, however, xenotime occurs, in the fractures and fissure track and is associated with apatite and rutile. Xenotime in the studied mineralized lamprophyre dykes is frequently homogeneous. Xenotime grains are present in the form of subhedral to anhedral crystals and range in size from 2 to 10 μm or 5 to 30 μm (Figs. 4a, b). The average contents of major oxides in xenotime (Table 2), obtained by the EPMA analysis, are: P_2O_5 (34.87 wt%), Y_2O_3 (34.11 wt%), Yb_2O_3 (6.21 wt%), Er_2O_3 (5.30 wt%), Dy_2O_3 (2.31 wt%), Ho_2O_3 (0.92 wt%), Tm_2O_3 (0.7 wt%), Tb_2O_3 (0.47 wt%), UO_2 (1.13 wt%), ThO_2 (0.79 wt%). The results of EPMA analysis showed that the studied xenotime is enriched in HREE (especially Yb, Er, Dy, Gd), Y, Th, and U (Table 2).

Table 1. Composition of selected monazite from the Abu Rusheid lamprophyre dyke, obtained by EPMA

Sample no.	**M 1**	**M 2**	**M 3**	**M 4**	**M 5**	**M 6**	**M 7**	**M 8**	**Average**	**Average**
Mineral	**Monazite**	**Monazite**	**Monazite**	**Monazite**	**Monazite**	**Monazite**	**Monazite**	**Monazite**	**Monazite**	**Monazite**
Oxides (wt%)	**dark**	**light**	**dark**	**light**	**dark**	**light**	**dark**	**light**	**dark**	**light**
	M 1	M 2	M 3	M 4	M 5	M 6	M 7	M 8	**N=4**	**N=4**
Al_2O_3	0.82	0.03	0.13	0.25	0.11	0.22	1.0	0.03	0.51	0.13
SiO_2	0.29	0.53	0.24	0.19	0.20	0.17	0.35	0.24	0.27	0.28
CaO	5.19	5.03	5.82	4.58	5.49	4.00	6.22	6.01	6.18	4.91
Y_2O_3	12.98	9.25	7.30	6.99	9.06	8.72	8.43	7.01	9.94	7.99
P_2O_5	23.0	20.4	25.3	23.9	25.7	24.3	26.1	23.9	25.5	23.6
La_2O_3	3.46	5.99	3.02	3.78	3.25	3.30	4.23	6.15	3.49	4.81
Ce_2O_3	2.31	10.52	15.33	15.42	16.37	14.33	2.82	10.18	9.21	12.86
Pr_2O_3	5.15	4.58	4.78	4.68	3.97	4.08	6.30	3.46	5.05	4.20
Nd_2O_3	15.35	16.10	16.73	15.91	13.72	13.01	16.77	17.12	16.14	15.54
Sm_2O_3	3.75	2.96	0.000	2.106	0.000	0.966	4.59	1.28	2.09	1.58
Eu_2O_3	0.00	0.00	0.00	0.00	0.00	0.00	0.00	0.00	0.00	0.00
Gd_2O_3	3.94	3.56	4.75	4.01	3.94	2.91	3.82	3.45	4.11	3.49
Dy_2O_3	6.16	6.09	5.45	5.05	6.18	6.15	5.54	5.12	5.83	5.60
PbO	0.50	1.1	0.35	0.66	0.29	0.58	0.61	1.28	0.43	0.90
ThO_2	0.02	0.42	0.21	0.42	0.09	0.81	0.02	0.30	0.08	0.49
UO_2	0.97	0.92	0.86	2.91	0.71	2.54	1.08	1.18	0.93	1.86
Total	83.87	87.48	90.30	90.91	89.06	86.04	87.89	86.68	87.78	87.78
Cation proportions (based on 4 oxygen atoms)										
Al	0.026	0.001	0.003	0.007	0.004	0.008	0.031	0.001	0.016	0.004
Si	0.009	0.017	0.006	0.005	0.008	0.006	0.011	0.008	0.009	0.009
Ca	0.130	0.126	0.145	0.100	0.137	0.115	0.156	0.150	0.281	0.223
Y	0.270	0.193	0.189	0.182	0.152	0.146	0.217	0.146	0.207	0.167
P	0.718	0.638	0.792	0.748	0.802	0.811	0.816	0.746	0.912	0.844
La	0.072	0.125	0.068	0.069	0.063	0.079	0.088	0.128	0.073	0.100
Ce	0.048	0.219	0.319	0.299	0.319	0.289	0.059	0.212	0.192	0.268
Pr	0.107	0.095	0.083	0.085	0.100	0.098	0.131	0.072	0.105	0.088
Nd	0.320	0.335	0.348	0.331	0.286	0.271	0.349	0.357	0.336	0.324
Sm	0.078	0.062	0.000	0.020	0.000	0.023	0.096	0.027	0.044	0.033
Gd	0.082	0.074	0.082	0.061	0.099	0.084	0.080	0.072	0.086	0.073
Dy	0.128	0.127	0.129	0.128	0.114	0.105	0.115	0.107	0.122	0.117
Pb	0.005	0.011	0.003	0.006	0.004	0.007	0.006	0.013	0.005	0.009
Th	0.001	0.008	0.004	0.008	0.002	0.026	0.001	0.004	0.030	0.033
U	0.016	0.016	0.015	0.049	0.012	0.015	0.018	0.020	0.016	0.032
∑REE	40.12	49.8	46.43	44.78	53.06	50.96	44.07	46.77	45.92	48.08
∑REE+Y	53.1	59.05	55.49	53.5	60.36	57.95	54.5	53.78	55.86	56.18
∑LREE	30.02	40.15	36.31	34.72	42.86	41.90	34.71	38.19	35.98	38.74
∑HREE	10.1	9.65	10.12	9.09	10.2	9.06	9.36	8.58	9.95	9.10
Th / U	0.02	0.46	0.24	0.07	0.13	0.32	0.02	0.25	0.04	0.28
∑A+B	2.01	2.09	2.16	2.08	2.15	2.04	2.19	2.08	2.13	2.07

N= number of samples

Table 2. Composition of selected xenotime from the Abu Rusheid lamprophyre dyke, obtained by EPMA

Sample no.	X 1	X 2	X 3	X 4	X 5	Average
Mineral	Xenotime	Xenotime	Xenotime	Xenotime	Xenotime	Xenotime
Oxides (wt%)						N=5
Al_2O_3	0.42	0.68	0.000	0.000	0.000	0.22
SiO_2	1.33	1.32	2.22	2.98	1.01	1.77
As_2O_3	0.05	0.19	0.00	0.00	0.00	0.04
CaO	0.16	0.64	0.01	0.05	0.05	0.18
Y_2O_3	30.92	41.24	33.99	31.72	32.67	34.87
P_2O_5	31.36	41.41	34.35	33.12	34.12	34.11
ZrO_2	0.04	0.16	0.00	0.35	0.36	0.18
Nb_2O_5	0.48	0.93	0.00	0.00	0.00	0.28
Nd_2O_3	0.10	0.38	0.31	0.13	0.13	0.19
Sm_2O_3	0.00	0.00	0.00	0.21	0.22	0.09
Eu_2O_3	0.02	0.08	0.00	0.12	0.01	0.05
Gd_2O_3	0.00	0.00	0.45	0.21	1.67	0.47
Tb_2O_3	0.60	0.41	0.68	0.11	0.66	0.47
Dy_2O_3	3.35	1.39	1.97	1.62	3.22	2.31
Ho_2O_3	1.56	0.47	0.56	0.64	1.38	0.92
Er_2O_3	7.18	1.23	4.08	6.85	7.06	5.30
Tm_2O_3	0.31	0.23	0.42	1.34	1.41	0.70
Yb_2O_3	8.49	1.56	5.11	7.81	8.05	6.21
HfO_2	0.40	0.00	0.00	0.50	0.52	0.28
Ta_2O_5	0.00	0.12	0.00	0.55	0.56	0.25
PbO	0.06	0.40	0.45	0.43	0.45	0.36
ThO_2	0.12	0.30	1.12	1.18	1.22	0.79
UO_2	0.95	0.99	1.25	1.21	1.24	1.13
Total	88.00	93.90	87.07	91.12	96.00	91.22
Cation proportions (based on 4 oxygen atoms)						
Al	0.015	0.024	0.000	0.000	0.000	0.008
Si	0.042	0.041	0.069	0.093	0.032	0.055
As	0.001	0.004	0.000	0.000	0.000	0.001
Ca	0.007	0.029	0.001	0.002	0.002	0.008
Y	0.644	0.859	0.708	0.661	0.681	0.711
P	0.782	1.03	0.859	0.828	0.853	0.816
Zr	0.001	0.003	0.000	0.007	0.008	0.004
Nb	0.010	0.019	0.000	0.000	0.000	0.006
Nd	0.002	0.008	0.006	0.003	0.003	0.004
Sm	0.000	0.000	0.000	0.004	0.005	0.002
Eu	0.001	0.017	0.000	0.003	0.001	0.004
Gd	0.000	0.000	0.009	0.004	0.035	0.010
Tb	0.013	0.009	0.014	0.001	0.014	0.010
Dy	0.07	0.029	0.041	0.034	0.067	0.048
Ho	0.032	0.01	0.012	0.013	0.029	0.019
Er	0.15	0.026	0.087	0.143	0.147	0.111
Tm	0.006	0.000	0.009	0.028	0.029	0.014
Yb	0.177	0.033	0.106	0.163	0.168	0.129
Hf	0.008	0.000	0.000	0.011	0.011	0.004
Ta	0.000	0.002	0.000	0.011	0.012	0.005
Pb	0.001	0.008	0.009	0.009	0.009	0.007
Th	0.002	0.061	0.02	0.022	0.022	0.025
U	0.016	0.017	0.021	0.021	0.021	0.019
∑HREE	21.58	5.54	13.67	19.15	23.8	16.75
∑HRE+Y	52.5	46.78	47.66	50.87	56.47	50.86
Th / U	1.06	1.29	2.37	2.38	2.46	1.91
Zr / Hf	0.44	0.16	0.00	0.86	0.88	0.47
∑A+B	1.91	2.18	1.96	2.04	2.08	2.03

N = number of samples

Xenotime and monazite stability

The studied monazite is strongly zoned, as observed by SEM. According to Heinrich et al. (1997), prograde zoning of metamorphic monazite and the partitioning of REE between monazite and xenotime are a function of temperature and pressure. It would appear that the U-Th partitioning between coexisting monazite and xenotime is also temperature and pressure dependent and that crystals might be zoned in respect to their U/Th ratios. Xenotime can thus be used as a sensitive trace element geothermometer, both within monazite-xenotime pair (Andrehs & Heinrich, 1998). The data obtained by EPMA analyses of the studied monazite-(Nd) and xenotime-(Y) were plotted on the $CePO_4$-YPO_4-$ThSiO_4$ ternary system at different temperatures (Fig. 8), according to Gratz & Heinrich (1997) and Seydoux-Guillaume et al. (2002). It can be inferred from the diagram that the studied xenotime from Abu Rusheid lamprophyre dyke formed at a temperature around 600 °C, while monazite formed at temperatures between 600 and 1100 °C (Fig. 8).

REE bearing minerals

Apatite ($Ca_{10}(PO_4)_6F_2$)

Apatite mainly occurs in the form of massive, euhedral to subhedral grains with size ranging from 10 to 40 μm (Figs. 4a, d, e, 5a). The apatite crystals are generally light gray to black in color under the transmitted light of an optical microscope (Figs. 3d - f). Chemical composition of apatite, obtained by EPMA, corresponded to fluorapatite (Table 3). The EPMA analyses (Table 3) also showed that the contents of major oxides and elements in the core of fluorapatite are: CaO (52.93 to 56.6 wt%), P_2O_5 (39.78 to 42.12 wt%), and F (3.18 to

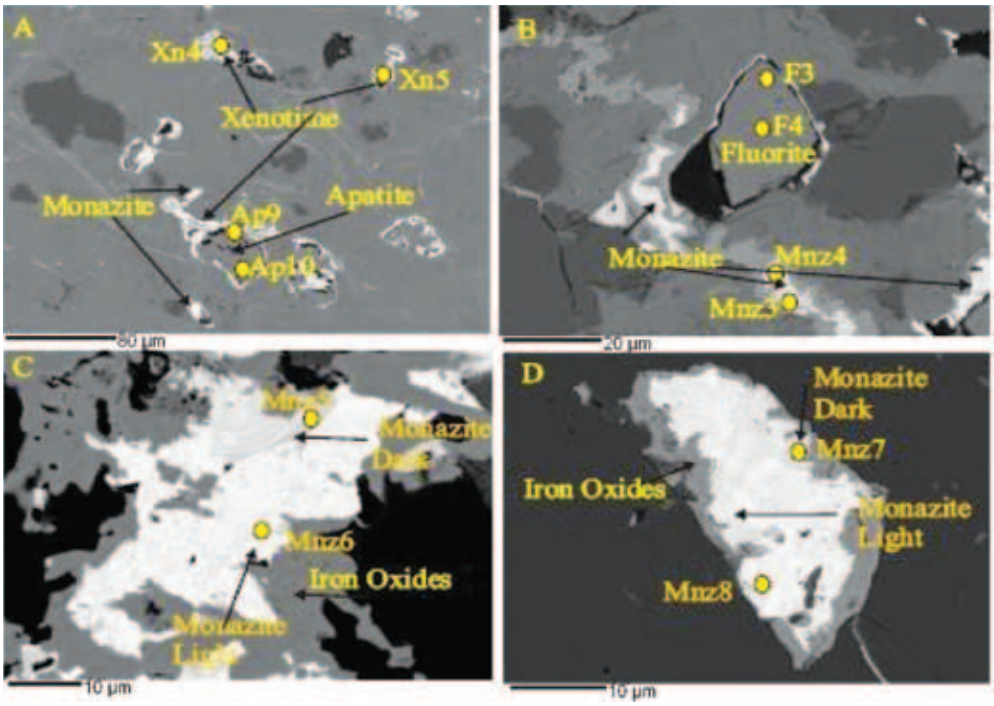

Fig. 5. SEM-BSE images of a) apatite altered and breakdown to xenotime and monazite on the rim of apatite b) fluorite rimmed by monazite and xenotime on a rime, c) and d) heterogeneous monazite grain with darker and lighter parts, associated with iron oxides.

4.15wt %), while in the rim of fluorapatite their values are: CaO (54.97 to 57.2 wt%), P_2O_5 (38.66 to 42.39wt %), and F (3.55 to 3.7wt %). Minor amounts of LREE, Y, Fe, U, Sr and Si were also found as substituents in apatite, especially in the rim of apatite (Fig. 5b, Table 3). Uranium usually substitutes for Ca in apatite.

As pointed out by Zhu & Sverjensky (1991), the formation of apatite with a composition of environments is F-rich, even though the activity of Cl in the fluid is much higher than that of F. The formation of the studied apatite is similar. In some carbonatitic apatite (Hogarth, 1989), F appears to overfill the site, especially when significant CO_3^{2-} is present (Piccoli & Candela, 2002). However, carbonatitic apatite contains very high Sr (commonly > 2500 ppm) and low Y contents (commonly < 400 ppm) (Belousova et al., 2002). The EPMA data (Table 3) show that studied apatite from the Abu Rusheid lamprophyre dykes are similar to other Kiruna type apatite occurrences and would seem to exclude a carbonatitic affinity.

Zircon ($ZrSiO_4$)

Zircon is found as the most abundant accessory mineral in the studied lamprophyre dykes of the Abu Rusheid area. Zircon occurs as subhedral prismatic to anhedral crystals of 20 to 50 μm in size. In the studied dykes, zircon is characterized by inclusions of xenotime and monazite (Figs. 4e, f). The core of zircon in the mineralized lamprophyre dyke contains inclusions of xenotime and monazite but has lower Hf and HREE contents than the rim of the studied zircon. Zircon crystals in the studied mineralized granites are mainly characterized by considerable metamictization, due to presence of uranium. The EPMA analyses of these crystals confirmed the zircon composition (Table 4). The EPMA analyses of these crystals confirmed the zircon composition (Table 4). The EPMA analyses (Table 4) indicate that the major oxides in the core of zircon are ZrO_2 (59.93 to 65.22 wt%), SiO_2 (31.71 to 33.12wt %), HfO_2 (0.89 to 1.23 wt%), and HREE (0.36 to 0.47 wt%) with significant amounts of ThO_2 (0.32 to 0.34 wt%), UO_2 (0.022 to 0.84wt %), FeO (0.03 to 2.18wt %), and Y_2O_3 (0.14 to 0.43 wt%). In the rim of zircon, contents of major oxides are mainly ZrO_2 (40.86 to 64.93 wt%), SiO_2 (23.55 to 34.70 wt%), HfO_2 (1.77 to 2.15wt %), and HREE (2.73 to 3.12 wt%) with significant amounts of ThO_2 (0.03 to 2.91 wt%), UO_2 (0.21 to 2.21 wt%), FeO (0.14 to 1.59 wt%), and Y_2O_3 (8.89 to 9.47 wt%) in (Table 4).

Fluorite (CaF_2)

The fluorite occurs as large euhedral to subhedral crystals with sizes ranging from 10 - 40 μm (Figs. 4b, 5b). Fluorite is commonly associated with zircon and thorite. The presence of fluorite accompanying the mineralization indicates alteration processes due to hydrothermal activity. The EPMA analyses (Table 5) indicate that the major oxides and elements in fluorite are CaO (68.75 wt%), and F (45.83 wt%). Significant amounts of Y_2O_3 (2.7 wt%), REE (2 wt %), Ce_2O_3 (0.7 wt%), ThO_2 (0.2 wt%), and UO_2 (0.02 wt%), were also found in fluorite Ce, Y, U, Th, and REE probably occur as substitutions in fluorite.

Rutile (TiO_2)

Rutile was only found as a small crystal in the lamprophyre dyke in the Abu Rusheid area, which contains inclusions of xenotime. Generally, it is altered to xenotime in the fissure tracks of the rutile (Fig. 4c).

Table 3 Composition of selected apatite from the Abu Rusheid lamprophyre dyke, obtained by EPMA

Sample no.	A1	A2	A3	A4	A5	A6	A7	A8	Average	Average
Mineral	Apatite	Apatite	Apatite	Apatite	Apatite	Apatite	Apatite	Apatite	Core	Rim
Oxides (wt%)	Core	Rim	Core	Rim	Core	Rim	Core	Rim	N=4	N=4
F	3.68	3.18	3.58	3.92	3.55	3.61	3.7	4.15	3.63	3.72
SiO_2	0.24	0.42	0.12	0.16	0.08	0.16	0.12	0.19	0.14	0.23
MgO	0.01	0.07	0.02	0.04	0.00	0.00	0.03	0.04	0.01	0.04
CaO	55.38	54.97	56.60	57.20	55.65	53.99	56.38	52.93	56.00	54.77
P_2O_5	40.96	38.66	41.81	42.39	42.12	39.48	42.4	39.78	41.82	40.08
Cl	0.00	0.00	0.00	0.00	0.00	0.01	0.00	0.00	0.00	0.00
FeO	0.46	0.63	0.51	0.48	0.49	0.71	0.49	0.66	0.49	0.62
SrO	0.45	0.09	0.09	0.10	0.08	0.03	0.09	0.03	0.18	0.06
Y_2O_3	0.00	0.38	0.00	0.00	0.40	0.63	0.00	1.23	0.10	0.56
La_2O_3	0.23	0.00	0.06	0.09	0.06	0.16	0.07	0.00	0.11	0.06
Ce_2O_3	0.28	0.00	0.05	0.16	0.00	0.09	0.03	0.00	0.09	0.06
Pr_2O_3	0.03	0.11	0.15	0.09	0.08	0.04	0.00	0.00	0.06	0.06
Nd_2O_3	0.14	0.00	0.12	0.06	0.00	0.27	0.01	0.10	0.07	0.11
Sm_2O_3	0.14	0.00	0.00	0.00	0.00	0.00	0.00	0.00	0.03	0.00
Gd_2O_3	0.00	0.06	0.00	0.19	0.00	0.12	0.11	0.18	0.03	0.14
PbO	0.05	0.19	0.01	0.00	0.00	0.00	0.00	0.07	0.01	0.06
ThO_2	0.00	0.00	0.00	0.00	0.00	0.00	0.03	0.00	0.00	0.010
UO_2	0.18	0.13	0.02	0.14	0.00	0.05	0.18	0.22	0.10	0.13
Total	99.92	97.57	101.62	103.37	101.01	97.83	101.72	97.84	101.07	99.15
Cation proportions (based on 4 oxygen atoms)										
F	-----	-----	-----	-----	-----	-----	-----	-----	-----	-----
Mg	0.001	0.003	0.001	0.002	0.000	0.001	0.001	0.001	0.002	0.001
Si	0.007	0.013	0.031	0.005	0.002	0.005	0.004	0.006	0.011	0.007
P	1.01	0.967	1.05	1.06	1.05	0.987	1.05	0.999	1.04	1.00
Cl	-----	-----	-----	-----	-----	-----	-----	-----	-----	-----
Ca	0.938	0.948	0.976	0.986	0.959	0.931	0.972	0.913	0.961	0.945
Fe	0.014	0.020	0.016	0.015	0.015	0.022	0.015	0.021	0.015	0.020
Sr	0.016	0.004	0.003	0.004	0.003	0.001	0.003	0.001	0.006	0.003
Y	0.000	0.008	0.000	0.000	0.008	0.013	0.000	0.026	0.002	0.012
La	0.005	0.000	0.001	0.002	0.001	0.003	0.001	0.000	0.002	0.001
Ce	0.006	0.000	0.001	0.003	0.000	0.002	0.001	0.000	0.002	0.001
Pr	0.001	0.002	0.003	0.002	0.002	0.001	0.000	0.000	0.002	0.002
Nd	0.003	0.000	0.002	0.001	0.000	0.000	0.000	0.000	0.002	0.001
Sm	0.003	0.000	0.000	0.000	0.000	0.000	0.000	0.000	0.001	0.000
Gd	0.000	0.001	0.000	0.004	0.000	0.002	0.002	0.004	0.001	0.003
Pb	0.001	0.002	0.000	0.000	0.000	0.000	0.000	0.000	0.001	0.002
Th	0.000	0.000	0.000	0.000	0.000	0.000	0.001	0.000	0.000	0.001
U	0.003	0.002	0.001	0.002	0.000	0.001	0.003	0.004	0.002	0.002
LREE	0.81	0.172	0.371	0.588	0.145	0.681	0.218	0.283	0.39	0.99
LREE+Y	0.000	0.557	0.000	0.000	0.544	1.312	0.000	1.508	0.49	1.55

---- not calculated
N = number of samples

Iron oxides

Iron oxides are most common and very important in the mineralized lamprophyre dyke especially in the fractures and fissure tracks (Fig. 3f). They are associated with monazite, xenotime, apatite, fluorite, zircon, and rutile with inclusions of xenotime.

Discussion

The field observation shows that the mineralized lamprophyre dyke cuts the mineralized shear zone of Abu Rusheid area. The NNW-SSE faults along the shear zone itself acted as channel ways for the movement and focusing of hydrothermal fluids. Consequently, the lamprophyre dyke was subjected to the intense alteration processes (ferrugination, fluoritization, and carbonatization), brecciation and mineralization.

The mixing of volatile fluids with meteoric water and fluid-wall rock interactions caused changes in pH and oxygen activity and resulted in deposition of base metals. Precipitation of iron oxides probably decreased the pH of the solution thus giving rise to acidic fluids. The sudden

Table 4. Composition of selected zircon from the Abu Rusheid lamprophyre dyke, obtained by EPMA

Sample no.	Z1	Z2	Z3	Z4	Z5	Z6	Average	Average
mineral	Zircon	Zircon	Zircon	Zircon	Zircon	Zircon	Zircon	Zircon
Oxides (wt%)	Core	Rim	Core	Rim	Core	Rim	Core N=3	Rim N=3
SiO_2	31.71	34.72	32.68	23.55	33.12	31.97	32.50	30.08
ZrO_2	59.93	40.86	61.46	43.59	65.22	64.93	62.20	49.79
HfO_2	0.89	1.77	1.12	2.15	1.23	2.02	1.08	1.98
P_2O_5	0.18	0.61	0.43	0.47	0.29	0.56	0.30	0.55
CaO	0.34	2.24	0.34	2.09	0.01	1.44	0.23	1.92
FeO	1.82	1.60	2.18	0.99	1.03	1.14	1.67	1.24
Y_2O_3	0.15	8.89	0.43	9.47	0.31	6.89	0.30	8.42
Ce_2O_3	0.09	0.85	0.03	1.09	0.06	0.08	0.06	0.68
Tb_2O_3	0.00	0.08	0.00	0.15	0.05	0.25	0.02	0.16
Dy_2O_3	0.11	1.47	0.24	0.96	0.02	0.09	0.13	0.84
Yb_2O_3	0.25	1.67	0.07	1.77	0.02	0.43	0.12	1.29
PbO	0.02	0.01	0.08	0.15	0.00	0.02	0.03	0.06
ThO_2	0.34	2.91	0.33	2.41	0.02	0.03	0.23	1.78
UO_2	0.84	2.21	0.71	2.16	0.10	0.22	0.55	1.53
Total	96.65	99.97	100.1	99.99	99.85	98.89	98.87	99.62
Cation proportions (based on 4 oxygen atoms)								
Si	0.991	1.085	1.021	0.736	1.035	0.999	1.02	0.94
Zr	0.936	0.638	0.960	0.681	1.02	1.01	0.97	0.78
Hf	0.012	0.024	0.015	0.029	0.017	0.020	0.015	0.024
P	0.005	0.015	0.011	0.012	0.000	0.001	0.005	0.009
Ca	0.009	0.062	0.009	0.058	0.000	0.000	0.006	0.04
Fe	0.057	0.050	0.068	0.031	0.001	0.001	0.042	0.027
Y	0.003	0.185	0.009	0.197	0.000	0.000	0.004	0.127
Ce	0.002	0.018	0.001	0.023	0.001	0.002	0.001	0.014
Tb	0.000	0.002	0.000	0.003	0.001	0.000	0.001	0.002
Dy	0.002	0.031	0.005	0.002	0.001	0.000	0.003	0.011
Yb	0.005	0.035	0.002	0.037	0.000	0.009	0.002	0.027
Pb	0.001	0.001	0.001	0.002	0.000	0.001	0.001	0.001
Th	0.006	0.053	0.006	0.044	0.001	0.001	0.004	0.036
U	0.014	0.038	0.012	0.037	0.002	0.004	0.009	0.026
Zr/ Hf	67.41	23.10	54.68	20.30	53.02	45.41	58.37	29.60
Th / U	0.41	1.32	0.47	1.11	0.23	0.14	0.37	0.857
ΣA+B	2.04	2.28	2.10	1.89	2.08	2.05	2.07	2.07

N = number of samples

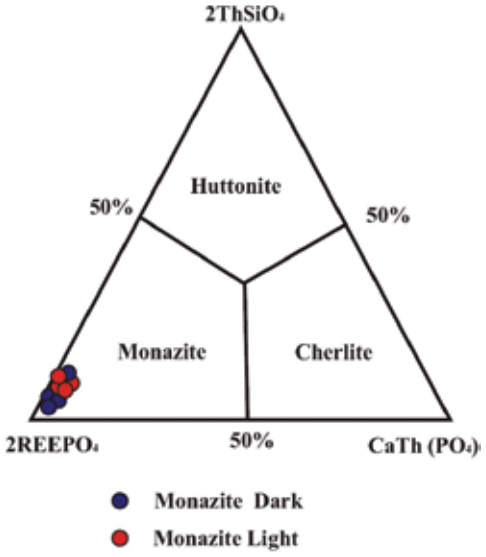

Fig. 6. Nomenclature diagram for the system monazite ($2REEPO_4$), cheralite ($CaTh(PO_4)$) and huttonite ($2ThSiO_4$) (after Linthout, 2007).

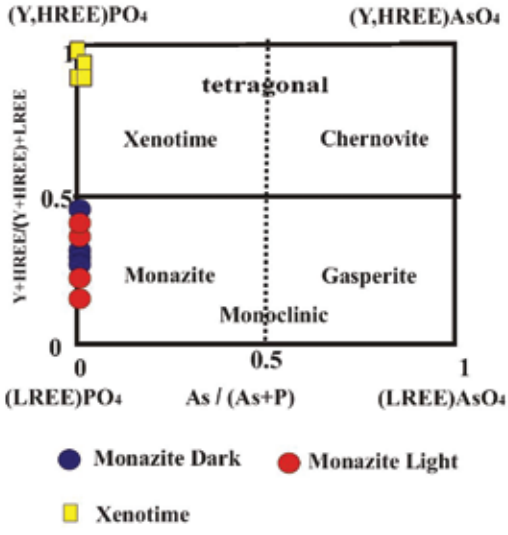

Fig. 7. Compositions of monazite–gasparite and xenotime-chernovite solid solutions in quadrilateral classification diagram of the $(Y,REE)AsO_4$-$(Y,REE)PO_4$ system (after Ondrejka et al., 2007).

Table 5. Composition of selected fluorite from the Abu Rusheid lamprophyre dyke, obtained by EPMA

Sample no.	F1	F2	F3	F4	Average	Average
Mineral	Flourite	Flourite	Flourite	Flourite	Core	Rim
Oxides (wt%)	Core	Rim	Core	Rim	N=2	N=2
F	46.21	44.43	44.87	39.80	45.54	42.12
Na_2O	0.93	0.46	0.32	0.12	0.62	0.29
Al_2O_3	0.46	1.46	0.46	2.25	0.46	1.86
SiO_2	0.81	0.46	1.40	0.65	1.11	0.56
P_2O_5	0.16	1.48	0.29	2.51	0.23	1.99
CaO	67.72	64.85	64.43	59.97	66.08	62.41
FeO	0.87	2.65	0.47	1.59	0.67	2.12
Y_2O_3	0.63	3.19	0.06	2.16	0.35	2.68
La_2O_3	0.06	0.14	0.03	0.13	0.05	0.13
Ce_2O_3	0.72	0.61	0.37	0.14	0.55	0.38
Pr_2O_3	0.03	0.07	0.15	0.05	0.09	0.06
Nd_2O_3	0.12	0.11	0.11	0.05	0.12	0.08
Sm_2O_3	0.03	0.06	0.01	0.00	0.02	0.03
Eu_2O_3	0.02	0.01	0.00	0.00	0.01	0.00
Gd_2O_3	0.10	0.18	0.05	0.26	0.08	0.22
Dy_2O_3	0.12	0.22	0.11	0.22	0.11	0.22
Er_2O_3	0.24	0.41	0.05	0.13	0.15	0.27
Yb_2O_3	0.35	1.82	0.38	2.16	0.36	1.99
PbO	0.01	0.08	0.02	0.25	0.01	0.16
ThO_2	0.19	0.37	0.07	0.24	0.13	0.31
UO_2	0.13	0.23	0.10	0.13	0.11	0.18
Total	101.4	100.5	103.2	105.2	102.3	102.8
Cation proportions (based on 4 oxygen atoms)						
F	------	-----	-------	-------	------	------
Na	0.029	0.014	0.010	0.004	0.02	0.009
Al	0.009	0.030	0.010	0.047	0.01	0.039
Si	0.025	0.014	0.044	0.020	0.035	0.017
P	0.004	0.037	0.007	0.063	0.006	0.05
Ca	1.69	1.62	1.61	1.51	1.65	1.57
Fe	0.027	0.083	0.015	0.050	0.021	0.066
Y	0.013	0.066	0.001	0.045	0.007	0.056
La	0.001	0.003	0.001	0.003	0.001	0.003
Ce	0.015	0.013	0.008	0.003	0.012	0.008
Pr	0.001	0.001	0.003	0.001	0.002	0.001
Nd	0.003	0.002	0.002	0.001	0.003	0.002
Sm	0.001	0.001	0.001	0.000	0.001	0.001
Eu	0.001	0.001	0.000	0.000	0.001	0.001
Gd	0.002	0.004	0.001	0.005	0.002	0.005
Dy	0.002	0.005	0.002	0.005	0.002	0.005
Er	0.005	0.009	0.001	0.003	0.003	0.006
Yb	0.007	0.038	0.008	0.045	0.008	0.042
Pb	0.001	0.001	0.001	0.001	0.001	0.001
Th	0.004	0.007	0.001	0.004	0.003	0.006
U	0.002	0.004	0.002	0.002	0.002	0.003
∑HREE	0.80	2.63	0.59	2.77	0.69	2.70
∑REE	1.77	3.63	1.25	3.13	1.51	3.38
∑REE+Y	2.4	6.82	1.32	5.29	3.06	6.06
Th / U	0.32	0.60	0.17	0.37	0.25	0.49

----- not calculated
N = number of samples

change in the pH and temperature of the fluids lead to destabilization of base metal complexes favouring their deposition in the lamprophyre dykes (Alexandrov et al., 1985). The emplacement of the lamprophyre dykes in the host rocks was accompanied by high temperature and CO_2 and caused heating of the host rock. This lead to leaching of trace elements from minerals and their remobilization through the foliation, joints, fractures and shear zones, accompanied by hydrothermal solutions, rich in Cu, Y, Pb, W, V, Zn, and U. The rare-metals precipitated from saline and reduced fluids, originating from the two mica granites, in the form of sulfides due to cooling, fluid mixing and wall rock reactions (Ibrahim et al., 2007b). The lamprophyres, together with hydrothermal solutions and alterations, play an important role in the concentration and formation of the minerals in shear zones. The lamprophyres formed from CO_2-rich magma. The CO_2 is characterized by its ability to fix all mineralization. So the lamprophyres are considered as a chemical trap for mineralization (Ibrahim et al., 2007b).

Crystallization of fluorite, galena, and pyrite in the mineralized shear zone of Abu Rusheid area reflects the important role of F and S. Zr, Hf, Th, and Ti are typical high field strength elements (HFSE), which are generally considered immobile during hydrothermal water-rock interaction. Experimental and natural evidence, however, have demonstrated that Zr, Ti, and Th may become mobile especially in high-temperature magmatic or hydrothermal environments containing strong complexing agents such as F, S, and others (Keppler, 1993). The fact that F may play a prominent role in the hydrothermal mobilization of HFSE has been indicated for Zr, Th and REE (Moine & Salvi, 1999). Also, fluoride complexes, e.g., (Zr, F) $(REE, F_4)_3$, are known to be stable under hydrothermal conditions (Mineyev, 1963). The abundantly detected zircon and Th-bearing minerals, demonstrably of hydrothermal origin, can be attributed to the role of F-rich fluids. Thus, although Zr and Th are generally considered as highly immobile elements, the occurrence of zircon indicates that significant concentrations of Zr and Th can be transported via specified F-rich fluids.

Monazite associated with fluorapatite is poor in Th ($0.00 \leq ThO_2 \leq 1.1$ wt%), but usually rich in U ($0.3 \leq UO_2 \leq 2.5$ wt%), and the Th/U ratio is always lower than unity and ave-

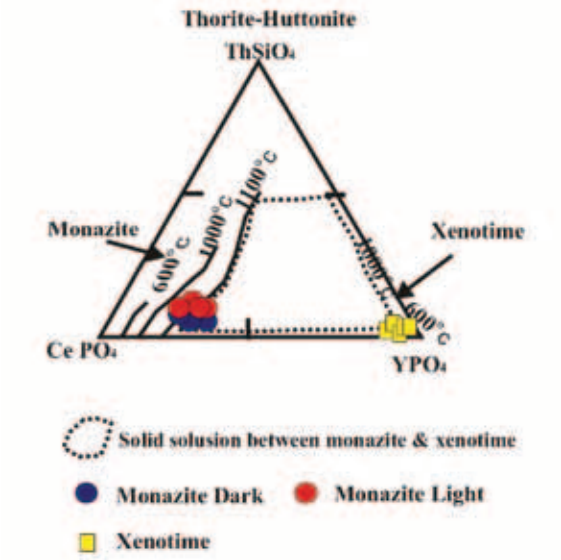

Fig. 8. Compositions of monazite and xenotime plotted in the $CePO_4$-$ThSiO_4$-YPO_4 ternary diagram (after Gratz & Heinrich,1997). Dashed lines represent monazite compositions at the respective temperatures at 200 MPa (Seydoux-Guillaume et al., 2002).

rages to 0.09. In this type of monazite, spatial relations and compositional features, suggest that the Th-poor, U-rich monazite-(Ce) formed as result of fluorapatite metasomatism (Ziemann et al., 2005). The studied monazite-(Nd) in the Abu Rusheid dyke, which is associated with fluorapatite, is poor in Th ($0.02 \leq ThO_2 \leq 0.81$ wt%) and rich in U ($0.92 \leq UO_2 \leq 2.91$ wt%), with the Th/U ratio always lower than unity, averaging 0.16. This indicates that monazite-(Nd) also formed as a result of flourapatite metasomatism.

Conclusions

1. The mineralized lamprophyre dyke in the Abu Rusheid area, occurs in a great fracture systems trending in NNW-SSE direction. It cuts cross the cataclastic mlyonite and mineralized granitic gneisses. The rocks are intruded by a huge intrusion of muscovite-biotite granites. The dyke in the Abu Rusheid area is characterized by HREE-minerals, such as xenotime-(Y) and monazite-(Nd), and REE-bearing minerals, such as apatite, fluorite, zircon, rutile with inclusions of xenotime and iron oxides.
2. The studied monazite-(Nd) in the lamprophyre dyke is frequently heterogeneous. There are two distinct parts in the same crystal. The part, which appears dark gray in BEI image, is enriched in HREE and depleted in LREE, Ca, Th and U, while the lighter gray part is depleted in HREE, Y and Ca and enriched in Th and U. The studied monazite is also characterized by low Th contents and shows strong zoning that reflects its hydrothermal origin.
3. The solid solutions between monazite and xenotime indicate that they formed at high temperatures from hydrothermal solutions. Composition of the studied monazite-(Nd) and xenotime-(Y), plotted on the $CePO_4$-YPO_4-$ThSiO_4$ ternary system indicated that the studied monazite and xenotime formed at a temperature around 600 °C.
4. The studied monazite-(Nd) in the Abu Rusheid dyke, which is associated with fluorapatite, is poor in Th ($0.02 \leq ThO_2 \leq 0.81$ wt%), but usually rich in U ($0.92 \leq UO_2 \leq 2.91$ wt%), and the Th/U ratio is always lower than unity and averages to 0.16. This indicates that the monazite formed as a result of flourapatite metasomatism. The event most likely responsible for metasomatism of the fluorapatite is documented by the associated monazite-(Nd).
5. Apatite was formed by magmatic fractionation and was affected by hydrothermal solutions enriched in REE, P and Y.
6. The emplacement of lamprophyre dykes within the mineralized shear zones was accompanied by high temperatures and CO_2. Presence of hydrothermal solutions, heated by the lamprophyre dykes, caused leaching and remobilization of REE, P, Zr, F, Y, and Ti from minerals in the wall rocks, which were then re-precipitated as the REE-minerals monazite-(Nd) and xenotime-(Y) in the fractures and fissure tack in the apatite, fluorite, rutile, zircon and iron oxides. Fluorite and galena also indicate the displacement of REE, P and Y by hydrothermal solution and re-deposition in the fracture and fissure tack in the apatite, fluorite, rutile, zircon and iron oxide minerals.
7. The studied lamprophyre dyke in the Abu Rusheid area contains high concentrations of REE, P, U, F, Zr, Ti, and Fe, especially in the form of HREE minerals, such as xenotime-(Y), monazite-(Nd, and REE-bearing apatite, fluorite, zircon, and rutile with inclusions of xenotime. Accordingly, the mineralized lamprophyre dyke in the Abu Rusheid area could represent a very good source of REE-minerals, especially HREE.

Acknowledgments

The author wishes to thank Dr. Douglas Hall and Prof. Dr. David Lentz, for their assistance and providing SEM and EPMA analyses at University of New Brunswick (UNB), Canada. The electron probe microanalyses were carried out during my post-doctoral fellowship at the University of New Brunswick (UNB), Canada.

References

Abadalla, H. M., Helba, H. & Matsueda, H. 2008: Chemistry of zircon in rare metal granitoids and associated rocks, Eastern Desert, Egypt, Resource Geology, 59/1: 51-68, doi:10.1111/j.1751-3928.2008.00079.x.

Abdel-Monem, A. A. & Hurley, P. M. 1979: U-Pb dating of zircons from psammitic gneisses, Wadi Abu Rusheid-Wadi Sikeit area, Egypt. Inst. Applied. Geology, Jeddah, Bull., 3: 165-170.

Alexandrov, I. V., Krasov, A. M. & Kochnova, L. N. 1985: The effects of K, Na and F on rock-forming mineral assemblages and the formation of tantalo-niobate mineralization in rare-element granite pegmatites. Geochemistry International, 22: 85-92.

Ali, M. A. Lentz, D. R.& Hall, D.C. 2011: Mineralogy and geochemistry of Nb-, Ta-, Sn-, U-, Th-, and Zr-Bearing granitic Rocks from Abu Rusheid Shear Zones, South Eastern Desert, Egypt, Chinese Journal of Geochemistry, 30: 1-28.

Andrehs, G. & Heinrich, W. 1998: Experimental determination of REE distributions between monazite and xenotime: potential for temperature-calibrated geochronology. Chemical Geology, 149: 83-96, http://doi:10.1016/S0009-2541(98)00039-4.

Anthony, J. W., Bideaux, R. A., Bladh, K. W. & Nichols, M. C. 2000: Handbook of Mineralogy. Arsenates, Phosphates, Vanadates, Mineral Data Publishing, Tucson, IV: 680 p.

Bea, F. 1996: Residence of REE, Y, Th andU in granites and crustal protholiths; implications for the chemistry of crustal melts. J. Petrol., 37: 521-552.

Belousova, E. A., Griffin, W. L., O'Reilly, S. Y. & Fisher, N. I. 2002: Apatite as an indicator mineral for mineral exploration: trace-element compositions and their relationship to host rock type. Journal of Geochemical Exploration, 76: 45-69, doi:10.1016/S0375-6742(02)00204-2.

Bennett, J. D. & Mosley, P. N. 1987: Tiered-tectonics and evolution, Eastern Desert and Sinai, Egypt. In: Matheis, G. & Schandelmeier, H. (eds.) Current research in African Earth Sciences. Balkema, Rotterdam, 79-82.

Butler, C. A., Holdsworth, R. E. & Stachan, R. A. 1995: Evidence for Caledonian sinistral strike-slip motion and associated fault zone weakening, outerhebrides fault zone, NW Scotland. Journal of Geological Society, 152: 743-746, doi:10.1144/gsjgs.152.5.0743.

Dawood, Y. H. 2010: Mineral chemistry and genesis of uranyl minerals associated with psammitic gneisses, Abu Rusheid area, South Eastern Desert of Egypt. JKAU: Earth Sci., 21/1: 137-169, doi:10.4197/Ear.21-1.6.

Deer, W. A., Howie, R. A. & Zussman, J. 1966: An introduction to rock forming minerals. Longmans, London: 517 p.

El-Gemmizi, M. A. 1984: On the occurrence and genesis of mud zircon in the radioactive psammitic gneisses of Wadi Nugrus, Eastern Desert, Egypt. Journal University of Kawait (Sci.), 2: 285-294.

Förster, H. J. 2000: Cerite-(Ce) and thorian synchysite-(Ce) from Niederbobritzsch (Erzgebirge, Germany): implications for the differential mobility of Th and the LREE during granite alteration. Canadian Mineralogist, 38: 67–79, doi:10.2113/gscanmin.38.1.67.

Förster, H. J. 1998a: The chemical composition of REE-Y-Th-U rich accessory minerals in peraluminous granites of the Erzgebirge- Fichtelgebirge region, Germany, Part I: The monazite- (Ce)- brabantite solid solution series. Am. Mineral., 83: 259-272.

Förster, H. J. 1998b: The chemical composition of REE-Y-Th-U-rich accessory minerals in peraluminous granites of the Erzgebirge-Fichtelgebirge region, Germany, Part II: xenotime. Am. Mineral., 83: 1302-1315.

Fritz, H., Dallmeyer, D. R., Wallbrecher, E., Loizenbauer, J., Hoinkes, G., Neumayr, P. & Khudeir, A. A. 2002: Neoproterozoic tectonothermal evolution of the Central Eastern Desert, Egypt: A slow velocity tectonic process of core complex exhumation [J]. Journal of African Earth Sciences, 34: 137–155, doi:10.1016/S0899-5362(02)00014-3.

Gaines, R., Skinner, H.C.W., Foord, E., Mason, B. & Rosensweig, A. 1997: Dana's New Mineralogy, 8th Edition. John Wiley and Sons, New York: 1906 p.

Graeser, S. & Schwander, H. 1987: Gasparite-(Ce) and monazite-(Nd): two new minerals to the monazite group from the Alps. Schweizerische Mineralogische und Petrographische Mitteilungen, 67:103–113.

Gratz, R. & Heinrich, W. 1997: Monazite-xenotime thermobarometry: experimental calibration of the miscibility gap in the binary system $CePO_4$-YPO_4. Am. Mineral., 82: 772-780.

Greiling, R. O., El-Ramly, M. F., Rashwan, A. A. & Kamal El-Din, G. M. 1993: Towards a comprehensive structural synthesis of the (Proterozoic) Arabian Nubian Shield in Egypt. In: Thorweihe, U. & Schandelmeie, H. (eds.): Geoscient. Res. Northeast Africa. Balkema, Rotterdam, 15-19.

Greiling, R. O., Kröner, A., El-Ramly, M. F. & Rashwan, A. A. 1988: Structural relationships between the southern and central parts of the Eastern Desert of Egypt: details of a fold and thrust belt. In: El-Gaby, S. & Greiling, R. O. (eds.): The Pan-African belt of Northeast Africa and adjacent areas. Vieweg, Wiesbaden, 121–146.

Hanson, G. N. 1978: Application of trace elements to the petrogenesis of igneous rocks of granitic composition. Earth and Plantary Science Letters, 39: 26-43.

Hassan, M. A. 1973: Geology and geochemistry of radioactive columbite-bearing psammitic gneiss of Wadi Abu Rusheid. South Eastern Desert, Egypt [J]. Annal of Geoogical Survey 3: 207 p.

Hassan, M. A. 1964: Geology and Petrographical Studies of the Radioactive Minerals and Rocks in Wadi Sikait-Wadi El-Gemal Area, Eastern Desert, Egypt, M. Sc. Thesis, Cairo University: 165 p.

Heinrich, W., Andrehs, G. & Franz, G. 1997: Monazite-xenotime miscibility gap thermometry: I. An empirical calibration. Journal metamorphic Geology, 15: 3-17.

Hilmy, M.E., El-Bayoumi, R. M. & Eid, A. S. 1990: Geology, geochemistry and mineralization of

the psammitic gneiss of the Wadi Abu Rusheid, Eastern Desert, Egypt. J. African Earth Science, 11: 197–205, doi:10.1016/0899-5362(90)90088-V

Garth, D. D. 1989: Pyrochlore, apatite and amphibole: distinctive minerals in carbonatite. In: Bell, K. (ed.): Carbonatites Genesis and Evolution. Unwin Hyman, London, 105-148.

Humphris, S. E. 1984: The mobility of the REE in the crust. In Henderson, P. (ed.): REE Geochemistry [M]. Elsevier, Amsterdam, 317–342.

Ibrahim, I., Saleh, G. M., Amer, T., Mahmoud, F., Abu El Hassan, A., Ali, M. A., Azab, M. S., Rashed, M., Khaleal, F. & Mahmoud, M. 2004: Uranium and Associated Rare Metals Potentialities of Abu Rusheid Brecciated Shear Zone II, South Eastern Desert, Egypt [M]. Nuclear Materials Authority, Internal Report, Cairo: 182 p.

Ibrahim, I., Saleh, G. M., Hassan, M. A., El-Tokhi, M. M. & Rashed, M.A. 2007a: Geochemistry of lamprophyres-bearing Uranium Mineralization, Abu Rusheid Area, South Eastern Desert, Egypt [C]. The 10th Int. Min. Petr. & Metal. Eng. Conf. Mining, 41-55.

Ibrahim, I., Saleh, G. M. & Rashed, M.A. 2007b: Base Metal Mineralization in Lamprophyre Dyke at Abu Rusheid Area, South Eastern Desert, Egypt [C]. The 10th Int. Min. Petrol. & Metal. Eng. Conf. Mining, 31-40.

Jefferies, N. L. 1984: The distribution of the rare earth elements within the Carnmeneltis Pluton, Cornwall. Mineralogical Magazine, 49: 495-504.

Keppler, H. 1993: Influence of fluorite on the enrichment of high field strength trace elements in granitic rocks. Contribution to Mineralogy and Petrology, 114: 479-788.

Massau, M., Černý, P., Cooper, M. A., Chapman, R. & Grice, J. D. 2002: Monazite-(Sm), a new member of the monazite group from the Annie Claim #3 granitic pegmatite, southeastern Manitoba. Canadian Mineralogist, 40: 1649–1655.

Mineyev, D. A. 1963: Geochemical differentiation of the rare earth geochemistry (USSR), International Geochemistry, 12: 1129-1149.

Miyawaki, R. & Nakai, I. 1987: Crystal structures of rare-earth minerals. Rare Earths (Kidorui), 11:1-133.

Moghazi, A. M., Hassanen, M. A., Mohamed, F. H. & Ali, S. 2004: Late Neoproterozoic strongly peraluminous leucogranites, South Eastern Desert, Egypt-petrogenesis and geodynamic significance. Mineral. Petrol., 81/2: 19–41, doi:10.1007/s00710-003-0021-5.

Moine, B. & Salvi, S. 1999: Role of fluorine-rich fluids in the hydrothermal transport of "immobile" elements (Th, Zr, REE, Zl). Bull. De liaison de la Societe Francaise de Mineralogie et de Cristallographie (S. F. M. C.) 11: 90-92.

Ni, Y., Hughes, J. M. & Hughes, J. M. 1995: Crystal chemistry of the monazite and xenotime structures. American Mineralogist, 80: 21–26.

Ondrejka, M., Uher, P., Pršek, J. & Ozdín, D. 2007: Arsenian monazite-(Ce) and xenotime-(Y), REE arsenates and carbonates from the Tisovec-Rejkovo rhyolite, Western Carpathians, Slovakia: Composition and substitutions in the (REE,Y)XO4. Lithos, 95: 116–129, doi:10.1016/j.lithos.2006.07.019

Pabst, A. & Hutton, C. O. 1951: Huttonite a new monoclinic thorium silicate. Am. Mineral., 36: 60- 69.

Piccoli, P. M. & Candela, P. A. 2002: Apatite in igneous systems. In: Kohn, M. J. et al. (eds.): Phosphates: Geochemical, Geobiological, and Materials Importance. Reviews in Mineralogy and Geochemistry, 48, Mineralogical Society of America, Washington, D.C. 255-292.

Raslan, M. F. 2005: Mineralogy and physical upgrading of Abu Rusheid radioactive gneiss, South Eastern Desert, Egypt. The 9th International Mining, Petroleum, and Metallurgical Engineering Conference February, Faculty of Engineering- Cairo University, Mining 27: 43-52.

Raslan, M. F. 2008: Occurrence of Ishikawaite (Uranium-rich Samarskite) in the mineralized Abu Rusheid gneiss, South Eastern Desert, Egypt. International Geology Review 50/12: 1132-1140, doi:10.2747/0020-6814.50.12.1132

Rose, D. 1980: Brabantite, $CaTh[PO_4]_2$, a new mineral of the monazite group, N. Jahrb. Miner. Monatsh., 247-257.

Saleh, G. M. 1997: The potentiality of uranium occurrences in Wadi Nugrus area, South Eastern Desert, Egypt. Ph. D. Thesis, Mansuora University, 171 p.

Schandl, E. S. & Gorton, M. P. 2004: A textural and geochemical guide to the identification of hydrothermal monazite: Criteria for selection of samples for dating epigenetic hydrothermal ore deposits. Economic Geology, 99/5: 1027-1035, doi:10.2113/gsecongeo.99.5.1027.

Seydoux-Guillaume, A. M., Wirth, R., Heinrich, W. & Montel, J. M. 2002: Experimental determination of Thorium partitioning between monazite and xenotime using analytical electron microscopy and X-ray diffraction Rietveld analysis. Eur. J. Mineral., 14/5: 869-878, doi:10.1127/0935-1221/2002/0014-0869.

Zhu, C. & Sverjensky, D. A. 1991: Partitioning of FCl-OH between minerals and hydrothermal fluids. Geochimica et Cosmochimica Acta, 55:1837-1858.

Ziemann, M. A., Förster, H. J, Harlov, D. E. & Frei, D. 2005: Origin of fluorapatite–monazite assemblages in a metamorphosed, sillimanitebearingpegmatoid, Reinbolt Hills, East Antarctica. Eur. J. Mineral., 17: 567-579.